Overview of JT-60U Results for Development of Steady-State Advanced Tokamak Scenario

H. Takenaga[1] and the JT-60 Team

[1] Japan Atomic Energy Agency, Naka, Ibaraki-ken, 311-0193 Japan

e-mail contact of main author : takenaga.hidenobu@jaea.go.jp

Abstract. Recent JT-60U experimental results towards development of steady-state advanced tokamak scenario are presented with emphasis on extension of the operation regimes and improvement of physics understandings for the strong parameter linkage. Reduction of toroidal magnetic field ripple by installing ferritic steel tiles decreases the fast ion loss, and consequently enables to access new regimes due to increase in net heating power and confinement improvement attributed to the reduction of counter toroidal rotation. High $\beta_N \cdot HH_{98(y,2)}$ of 2.2 with $\beta_N \sim 2.3$ and $HH_{98(y,2)} \sim 1$ is sustained for 23.1 s significantly longer than the current diffusion time ($\sim 12\tau_R$) in the high β_p ELMy H-mode plasmas with a weak positive shear. This duration is extended to the time scale for enhancement of recycling owing to the decrease in wall-pumping rate. Successful recycling and density control is demonstrated for ~ 30 s in the enhanced recycling regime even with outgas from the wall by maximizing the divertor pumping in the high-density ELMy H-mode plasmas. High β_N (~ 4.2) exceeding no wall ideal limit is achieved at l_i = 0.8-1 in the high β_p ELMy H-mode plasmas with the large volume configuration close to the wall, which had so far suffered from the large toroidal field ripple. Small critical rotation velocity is found for suppressing RWM. NTM stabilization is also demonstrated by real time control of current profile using LHCD in the large volume configuration with a reduced heat load to the LH antenna. With small effects of the toroidal field ripple reduction, parameter linkage is investigated in the reversed shear (RS) plasmas with high bootstrap current fraction (f_{BS}) of ~ 0.7-1. In these plasmas, the duration is determined by ideal limit or slow ITB degradation in the linkage of current and pressure profiles. Physics studies also progress towards burning plasma control. The semi-global nature is observed in the ITB region both for high β_p mode and RS plasmas. Complete NTM suppression is demonstrated with misalignment of ECCD position less than about half of the island width. Fast ELM propagation to the main chamber wall is observed, and significant hydrogen retention in the main chamber wall is found. In the plasma-shadowed area underneath the divertor region, the averaged carbon deposition rate is significantly low, however, (H+D)/C retention rate is high (~ 0.8).

1. Introduction

The major objectives of the JT-60U project are to establish physics basis for ITER and to develop the steady-state advanced tokamak scenario leading to realization of an attractive fusion reactor. For the advanced tokamak plasma, high normalized beta (β_N) and high bootstrap current fraction (f_{BS}) are essential [1]. In JT-60U, "high β_p mode" plasmas with a weak positive magnetic shear and reversed shear ("RS") plasmas have been developed by utilizing both internal and edge transport barriers (ITB and ETB). In these plasmas, plasma performance is determined among strong parameter linkage between phenomena dominated in various time scales, such as MHD activity, confinement and transport, current diffusion and plasma wall interaction. Therefore, it is important to sustain high performance plasmas exceeding the time scale of related key issues.

JT-60U experiments in 2003-2004 focus on long sustainment of high performance plasmas exceeding the time scale of current diffusion by modifying the operation system for long pulse operation (≤ 65 s) and long pulse neutral beam (NB) heating (≤ 30 s) [2]. Recent JT-60U experiments in 2005-2006 emphasize further improvement of the plasma performance and enhancement of physics understandings for the strong parameter linkage. The target new domains for the improvement of the plasma performance are long sustainment of high β_N together with high confinement and achievement of high β_N above no wall ideal limit. Towards extension of the operation regimes to the new domains, ferritic steel tiles are installed inside the vacuum vessel to increase net heating power and to enhance the controllability of toroidal rotation by reducing toroidal field ripple. The plasma rotation is important for improving the confinement [3] and stabilizing the resistive wall mode appeared in the high β_N regime above no wall ideal limit. JT-60U has various NB injections, such as perpendicular, co and counter (ctr) tangential injections. However, ctr-toroidal rotation antiparallel to the plasma current due to the fast ion loss induced by the toroidal field ripple limits the controllability of the toroidal rotation. In this paper, recent JT-60U experimental results after the 20th IAEA Fusion Energy Conference [2] are reviewed with emphasis on the extension of the operation regimes and the improvement of the physics understandings for the strong parameter linkage in the advanced tokamak plasmas.

2. Installation of Ferritic Steel Tiles and Its Effects on L- and H-mode plasmas

Ferritic steel tiles (FSTs) are installed inside the JT-60U vacuum vessel to reduce the toroidal field ripple [4] based on success of Advanced Material Tokamak EXperiment (AMTEX) program in JFT-2M [5]. The FSTs are set in the low-field-side (LFS) above the outer baffle plates under the TF coils in place of graphite tiles as shown in Fig. 1 (a) and cover ~10% of the vacuum vessel surface. Figure 1 (a) also shows reduction of quasi-ripple well region [6] in the toroidal angle of 0-20 deg. after the FSTs installation. The FSTs have ingredient of 8%Cr, 2%W and 0.2%V [7] and their saturation magnetization is about 1.7 T at 573 K. The toroidal field ripple is reduced by a factor of about 4 at $R = 4.2$ m and $Z = 0.6$ m in the case of toroidal magnetic field (B_T) of 1.86 T as shown in Fig. 1 (b). Monte-Carlo simulations considering fully 3-D magnetic field structure using the F3D OFMC code [6] indicate that total absorbed power increases by ~ 30% at $B_T < 2$ T for the large volume configuration close to the wall, which had so far suffered from the large toroidal field ripple. The calculated absorbed power fraction for each NB injection at $B_T = 1.86$ T are shown in Fig. 2.

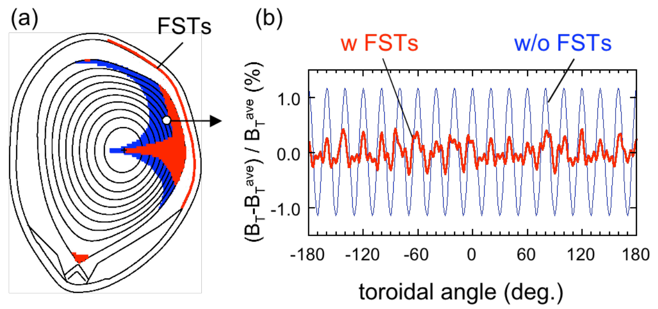

FIG. 1. (a) Poloidal position of FSTs (red line). Quasi-ripple well regions without (blue) and with (red) FSTs in the toroidal angle of 0-20 deg. at $B_T = 1.86$ T. (b) Toroidal variation of toroidal field strength at $R = 4.2$ m and $Z = 0.6$ m (circle in (a)) without (blue) and with (red) FSTs.

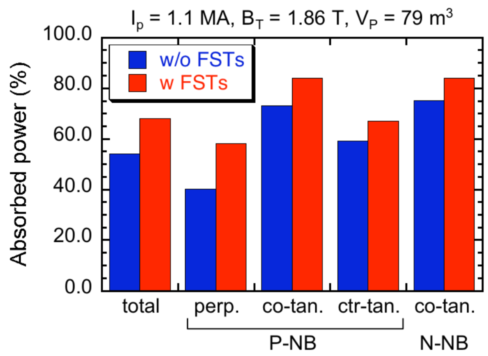

FIG. 2. Calculated absorbed power fractions without (blue) and with (red) FSTs for total and each NB injection (P-NB and N-NB : positive and negative ion based NB).

The heat load on the outer baffle plates is evaluated to be < 0.2 MW/m^2 based on IRTV measurement. This heat load level is comparable with the F3D OFMC calculation with the FSTs (< 0.3 MW/m^2) and significantly smaller than the calculation without the FSTs (> 1 MW/m^2), indicating reduction of the fast ion loss by installing the FSTs. The effects of the FSTs installation on toroidal rotation (V_T) and confinement are clearly observed [8, 9]. Reduction of the radial electric field attributed to decrease in the fast ion loss with the FSTs slows the ctr-rotation at the plasma edge. The edge V_T shifts to co-direction both with perp.

and co-NB injection in the large volume L-mode plasmas ($I_p = 1.2$ MA, $B_T = 2.6$ T, $q_{95} = 4.1$, $V_p = 75$ m^3) as shown in Fig. 3. In the H-mode plasmas with the same I_p, B_T, q_{95} and V_p, the V_T profile also becomes less counter with the FSTs. With changing pedestal V_T from ctr-direction to co-direction, the H-mode pedestal pressure increases as shown in Fig. 4 (a). Even at given pedestal V_T, the pedestal pressure is larger with the FSTs than without the FSTs. The linkage of the pedestal parameters is proposed in JT-60U [10]. The reduction of the toroidal field ripple could affect the linkage through not only the plasma rotation but also other mechanisms. The H-mode confinement is clearly improved with enhancing core V_T in co-direction for the large volume configuration as shown in Fig. 4 (b). The H-mode confinement is also improved by the reduction of toroidal field ripple at a given V_T.

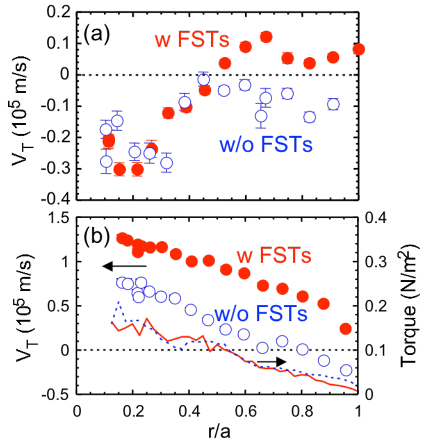

FIG. 3. V_T profiles w and w/o the FSTs for (a) perp. P-NB only and (b) co-P-NB in addition to perp. P-NB. Torque input is also plotted in (b) (w : solid, w/o : dotted line)

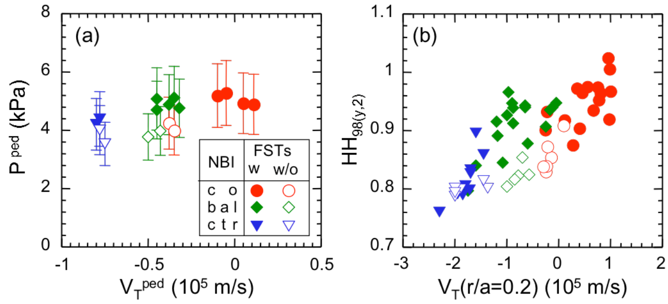

FIG. 4. (a) Pedestal pressure as a function of pedestal V_T. (b) $HH_{98(y,2)}$ as a function of central V_T. Various combinations of tan. P-NBs are applied in addition to pep. P-NBs.

3. Extension of Operation Regimes and Improvement of Controllability for Advanced Tokamak Plasmas by Utilizing Reduced Toroidal Field Ripple

The effects of the FSTs installation are investigated in long-pulse high β_p ELMy H-mode plasmas with ITB in relatively smaller volume configuration to achieve high β_N and high confinement simultaneously. Increase in net heating power and confinement improvement by reducing the fast ion loss allow to access high β_N regime in the large volume configuration. The JT-60U research area is extended to the regime above no wall ideal limit. The real time control for current profile is important for the advanced tokamak plasma due to strong parameter linkage including current profile. In JT-60U, the real time current profile control system has been developed using Motional Stark Effect (MSE) diagnostic and LH wave injection from LFS. The reduction of toroidal field ripple enables to demonstrate real time control in high β_N regime and to reduce heat load to the LH antenna located at LFS midplane.

3.1. Long Sustainment of High β_N and High Confinement Plasmas

In the heating duration from ~ 1-2 s to ~ 20 s, current diffusion plays key role to sustain high performance plasmas in addition to confinement/transport and MHD. In the high β_p ELMy H-mode plasma ($I_p = 0.9$ MA, $B_T = 1.6$ T and $q_{95} = 3.3$) with ITB, $HH_{98(y,2)} = 1$ as well as high β_N of 2.3 is sustained for 23.1 s (~ 12τ_R) [11] as shown in Fig. 5 (a). Here, the current diffusion time is defined as $\tau_R = \mu_0 \langle\sigma\rangle a^2/12$ [12]. The value of f_{BS} is estimated to be 36-45% and the current profile reaches steady state. In this discharge, neoclassical tearing mode (NTM) is suppressed by pressure profile control in the early phase and current diffusion does not affect the MHD activity. The thermal confinement is much improved compared with the

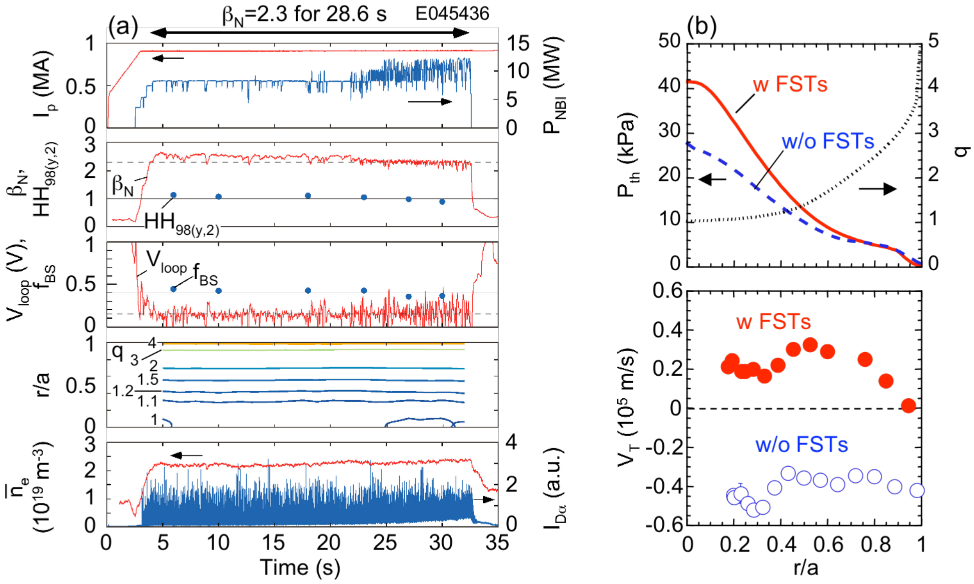

FIG. 5. (a) Waveforms of long high β_N and high $HH_{98(y,2)}$ discharge. (b) Comparison of thermal pressure and toroidal rotation profiles with (red) and without (blue) the FSTs.

high β_N discharges before the FSTs installation ($HH_{98(y,2)} = 0.71$). Figure 5 (b) shows comparison of the thermal pressure and V_T profiles before and after the FSTs installation at similar β_N. After the FSTs installation, high β_N is achieved with smaller heating power. The pedestal pressure is almost the same even with different V_T in contrast to the results for standard H-mode plasmas described in previous section. In JT-60U, the pedestal β_p is enhanced with increase in total β_p [10]. The toroidal rotation effect on the pedestal pressure might be small in the high β_p regime with ITB. The ITB is stronger after the installation than before the installation, which could be related to the change of the V_T profile. However, confinement degrades in the latter phase due to increase in the electron density (from $\bar{n}_e/n_{GW} = 0.47$ to 0.55) caused by enhancement of recycling, because the divertor pumping is insufficient to keep the low recycling level. Particle balance analysis indicates that the divertor pumping rate is smaller than the NB fuelling and enhancement of the recycling is ascribed to the change of wall pumping rate. The effect of the enhanced divertor pumping on the recycling and density is discussed in Section 6.1. After the FSTs installation, $\beta_N \cdot HH_{98(y,2)}$ is enhanced as shown in Fig. 6. Typically, $\beta_N \cdot HH_{98(y,2)} = 2.2$ is sustained for 23.1 s ($\sim 12\tau_R$), which is higher than that in the ITER baseline scenario (= 1.8) and close to ITER hybrid scenario.

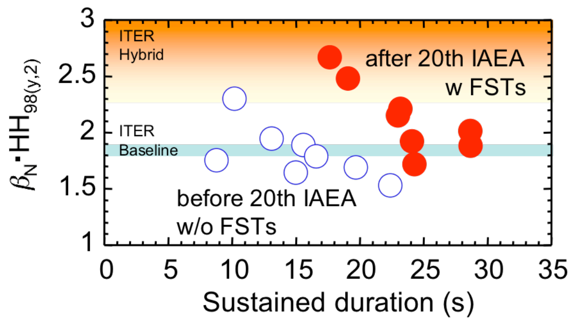

FIG. 6. $\beta_N \cdot HH_{98(y,2)}$ as a function of sustained duration. Closed and open symbols show the data with and without the FSTs, respectively.

3.2. High β_N Exceeding No Wall Ideal Limit and Effects of Plasma Rotation on Resistive Wall Mode

In the heating duration shorter than ~ 1-2 s, the high β_N are limited in the linkage of confinement/transport and MHD. High $\beta_N = 4.2$ exceeding no wall ideal limit is achieved in the high β_p ELMy H-mode plasmas at $I_p = 0.9$ MA, $B_T = 1.58$ T, $q_{95} = 3.56$ and $d/a \sim 1.2$ (d/a : ratio of radii at wall and plasma boundary) [13]. Figure 7 (a) shows achieved β_N as a function of internal inductance (l_i), which is a measure of no wall ideal limit, with and without the FSTs. Here, the data are plotted only for the large volume configuration ($V_p > 70$ m^3), where the wall stabilization effect is expected. In the range of $l_i = 0.8$-1, $\beta_N = 4.2$ ($= 4$-$5 \times l_i$) is achieved with the FSTs. Increase in net heating power and confinement improvement attributed to the reduction of ctr-rotation lead to achieve high β_N largely exceeding the no wall ideal limit. The resistive wall mode (RWM) stabilization by the plasma rotation also contributes to achieve the high β_N. The amplitude of RWM increases gradually with a slow time scale of several tens ms and the plasma rotation decreases at the same time. Then, the RWM amplitude increases rapidly with a time scale of several ms with the reduced plasma rotation. The time scale of the slow increase decreases with plasma rotation, indicating stabilizing effect of the plasma rotation on RWM. The achievable β_N is larger with co-rotation at the mode onset as shown in Fig. 7 (b), because β_N increases during the slow increase of the mode amplitude due to higher confinement. In order to clarify the plasma rotation effect on the RWM stabilization, the dependence of critical rotation velocity for suppressing RWM on C_β defined as $C_\beta = (\beta_N - \beta_N^{no\_wall})/(\beta_N^{ideal\_wall} - \beta_N^{no\_wall})$ is investigated with relatively smaller no wall ideal limit at lower l_i by utilizing enhanced toroidal rotation controllability. In this region, NB heating power is enough to increase β_N even with ctr-rotation. The value of β_N increases with ctr-NB, and ctr-NB is switched to co-NB to scan the rotation. The critical rotation velocity is estimated to be ~0.2% of alfvén velocity, which is smaller than that observed in DIII-D and JET [14]. The critical rotation velocity does not strongly depend on C_β as shown in Fig. 8.

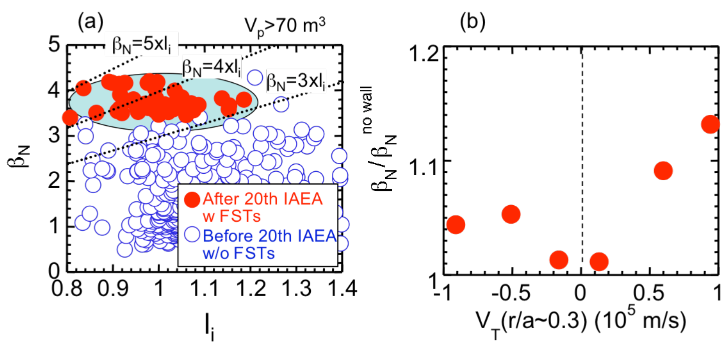

FIG. 7. (a) Achieved β_N as a function of l_i. Closed and open symbols show the data with and without FSTs. (b) Dependence of achievable β_N normalized by no wall ideal limit on toroidal rotation velocity at the mode onset.

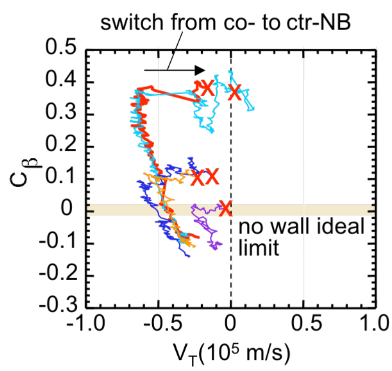

FIG. 8. Dependence of critical rotation velocity on C_β. Crosses show the disruption/collapse points.

3.3. Real Time Current Profile Control using LHCD

Steady attainable β_N is usually limited by NTM below the no wall ideal limit, when pressure gradient is significantly large at rational surfaces such as $q = 1.5$ or 2. The NTM stabilization techniques are developed using heating profile control and ECCD at rational surface. The NTM can be also stabilized when the minimum of safety factor (q_{min}) is raised above the corresponding values or rational surfaces move from the large pressure gradient zone by off-axis current drive. The real time current profile control system is developed, where the value of q_{min} is evaluated in real-time based on MSE signals and it controlled by LH wave power (P_{LH}) [15]. The value of P_{LH} is determined according to the following equation: $dP_{LH}/dt = -\alpha(q_{min}-q_{min,ref})$, where $q_{min,ref}$ is a reference value and α is the gain (positive value). Figure 9 shows waveforms in the high β_p ELMy H-mode plasmas (I_p = 0.8 MA, B_T = 2.4 T and P_{NB} = 14 MW), where q_{min} is controlled to stabilize NTM. When stored energy (W_{dia}) reached 1.55 MJ (β_N = 1.7, β_p=1.5), the m/n=2/1 NTM appeared, leading to decrease in W_{dia} by 22%. LH waves are injected from t = 7.5 s and real time control starts at t = 8 s with fixed phase of $\Delta\phi = 0^o$ (primary $N_{//} \sim 1.65$). The value of $q_{min,ref}$ is set to be 1.7 to move q = 2 rational surface from the large pressure zone. After the q_{min} control starts, P_{LH} increases and q_{min} reaches to 1.7 around t = 10 s. Then, P_{LH} is decreased by the control. The value of q_{min} exceeds the $q_{min,ref}$, and reaches to 2 at $t \sim 11$ s. The overshoot in q_{min} is caused by insufficient adjustment of the proportional gain of α = 0.3 MW/s. By increasing q_{min} to ~ 2, the m/n = 2/1 NTM is stabilized since q_{min} = 2 surface is eliminated or moved to the lower pressure gradient zone. After stabilization of NTM, W_{dia} starts to increase and recovers the initial value. The recovery of the confinement and β_N due to stabilization of NTM is demonstrated with current profile control.

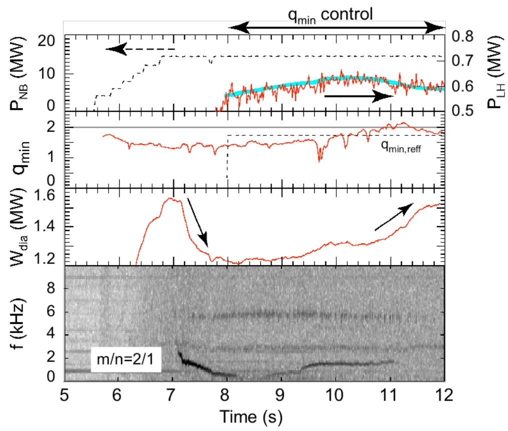

FIG. 9. Waveforms in the high β_p ELMy H-mode plasma with NTM stabilization using real time current profile control.

4. Development of Advanced Tokamak Plasma with High Bootstrap Current Fraction

High $f_{BS} \geq 0.7$ is required in a fusion reactor to reduce required current drive capability and center solenoid (CS) coil capability [1]. If it is possible to achieve bootstrap overdrive ($f_{BS} > 1$), this can be used for I_p ramp-up. In these plasmas, the current and pressure profiles strongly coupled. In order to develop the control scheme for such high f_{BS} plasmas, responses of these plasmas to internal parameter change and external perturbations are investigated in high B_T region (high q region) with small effect of toroidal field ripple reduction.

4.1. Long Sustainment of High Bootstrap Current Faction

In the RS plasma with a high bootstrap current fraction of ~ 75%, the evolution of inductive field is found to be largely affected by the change in bootstrap current [16], indicating strong linkage between pressure and current profiles. In this linkage, the plasma disrupts due to ideal MHD limit at q_{min} = 4 without pressure profile control for degradation of ITB. As shown in Fig. 10 (a), when pressure profile control at q_{min} = 4 ($t \sim 7$-8 s) is applied by changing the torque input (ctr-NB off), the disruption and the mini-collapse are avoided and high f_{BS} of ~ 70% is sustained for ~ 8 s with $HH_{98(y,2)} \sim 1.8$, $\beta_N \sim 1.4$ and $\beta_p \sim 2.1$ at I_p = 0.8 MA and B_T = 3.4 T ($q_{95} \sim 8.5$) [17]. In this discharge, stored energy feedback control is applied with constant reference value. In the later 3 s, q profile becomes flat with keeping the good ITB and is almost unchanged as shown in Fig. 10 (b). The radial profile of the time averaged internal loop voltage is flattened in time, indicating the current profile approaches steady state phase. However, mini-collapse occurs at $t \sim 13.3$ s. The density continues to increase until the mini-collapse, indicating the plasma profile does not reach steady state phase among the strong parameter linkage between pressure and current profiles. Effective pressure profile

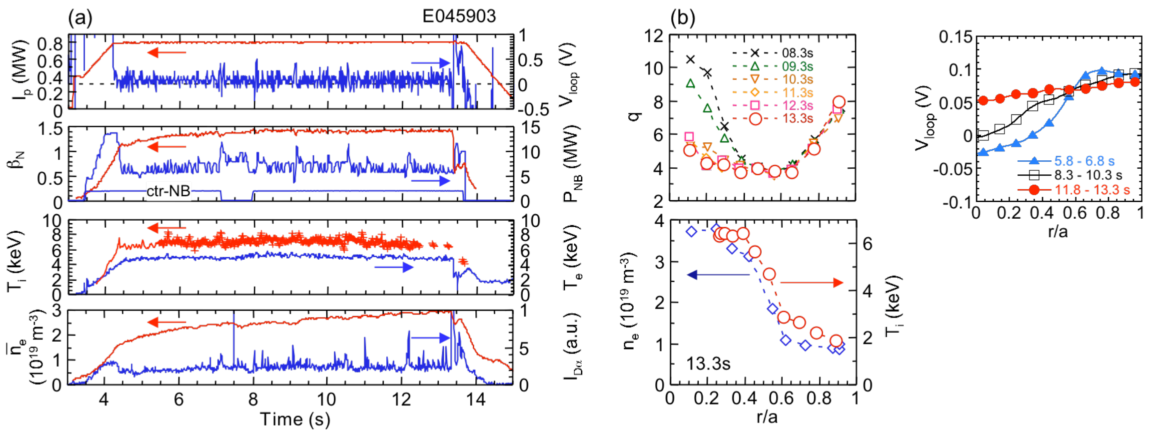

FIG. 10. (a) Waveforms of high f_{BS} (~ 70%) discharge and (b) profiles of q, n_e, T_i and V_{loop}.

control is required instead of global parameter control such as stored energy control even after the current profile approaches steady state to demonstrate long steady sustainment of high f_{BS} plasmas.

4.2. Bootstrap Current Sustained Plasmas

More attractive plasma operation regime is developed with a high f_{BS} close to unity. The behavior of fully bootstrap-driven and bootstrap-overdriven discharges is investigated in the RS plasmas with I_p = 0.5-0.6 MA and B_T = 3.7-4.0 T [18]. A typical bootstrap-sustained discharge is shown in Fig. 11. After inductive startup using the CS coil, the CS current is kept at a constant value after t = 4.2 s to prevent flux input by induction. Co-tangential NB is used during plasma startup, but is turned off at t = 4.1 s. Thereafter, I_p ramps up slightly and reaches a steady level at 0.54 MA. In this discharge the calculated NB driven current is approximately 50 kA in the ctr-direction. Therefore, I_p is almost sustained by the bootstrap current. The value of W_{dia} is maintained at a level of 1.05 MJ by feedback control of the NB power, corresponding to β_N = 1.15 and β_p = 2.72. This constant energy is maintained by increasing density and correspondingly decreasing electron and ion temperatures, indicating that both density and temperatures do not reach stationary states. In this discharge, no β collapse is observed, but the slow degradation of the energy confinement after t = 5 s leads to a slow decrease of W_{dia} and I_p. This plasma has a large safety factor of q_{95} = 13 and q_{min} = 10 at r/a ~ 0.8, and a current hole up to r/a ~ 0.3. Furthermore, the I_p ramp-up is clearly observed with the control for keeping the surface flux calculated in real time by Cauchy Condition Surface (CCS) method [19]. In this control scheme, the CS coil current is recharged to cancel the flux input due to increase in vertical field coil (VT and VR) for keeping plasma radial position constant in response to the increase in W_{dia}. During this

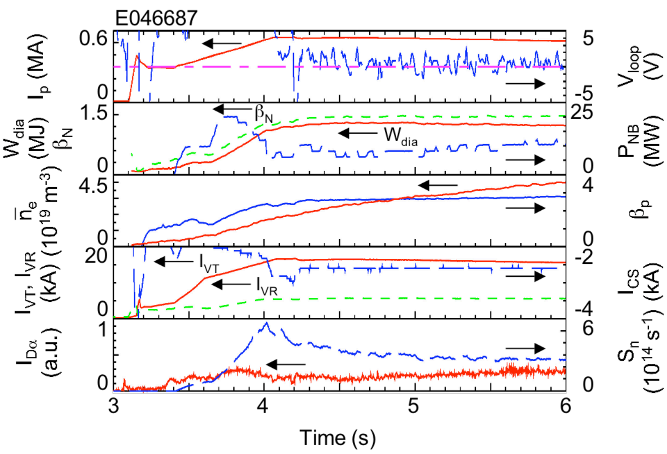

FIG. 11. A typical bootstrap-sustained discharge.

control scheme, I_p ramps up slowly at a nearly constant rate of 10 kA/s for about half a second.

5. Progress on Physics Studies towards Burning Plasmas

The physics studies are continued to resolve critical issues related to the control of burning plasmas with small effect of the reduction of toroidal field ripple. In this section, these are highlighted.

5.1. Transport Studies

5.1.1. Studies on Internal Transport Barrier

The ITB control is important issue for development of the advanced tokamak scenario as described in the previous sections. The degradation of ITB is observed in the ion temperature profile together with the flattering of the toroidal rotation profile, when EC wave is injected into the central region of the high β_p ELMy H-mode plasmas (I_p = 1.0 MA and B_T = 3.7 T) with both co- and ctr-rotation [20]. This degradation does not give fatal effect on ITB and the effect is retrievable, which is preferable for the ITB control. The effect is not sensitive to the deposition position of EC wave (see Fig. 12 (a)) and injection mode (CD mode or pure heating mode), indicating that this effect is semi-global nature of the ITB structure and current drive is not important. On the other hand, the ITB degradation is sensitive to I_p even with similar target ITB strength. In the high I_p regime, the EC wave injection is less effective. This is of great interest from viewpoints of both ITB physics and ITB control.

The semi-global nature is also observed during the ITB formation phase [21] in addition to the ITB-event [22]. The flattening of the temperature profile in the core region causes a narrower and stronger ITB in both high β_p ELMy H-mode and RS plasmas. In the RS plasma, a spontaneous phase transition from a wide and weak ITB (small χ_e at inner and large χ_e at outer) to a narrow and strong ITB (large χ_e at inner and small χ_e at outer), and back transition are observed on the transport time scale (~ 0.1-0.2 s) as shown in Fig. 12 (b). This behavior could make the burn control difficult by coupling to the change of α particle heating. In fact, in burn control simulation experiments with α particle heating simulation, whose power is determined proportionally to the DD neutron yield rate, a large variation of the external NB power is required for keeping the stored energy constant [23].

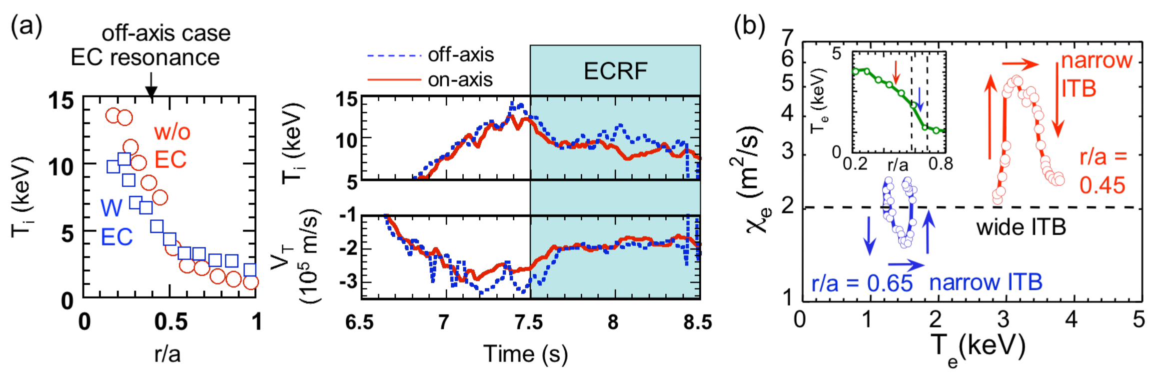

FIG. 12. (a) Response of T_i ITB to on- and off-axis EC wave injection in the high β_p ELMy H-mode plasmas. (b) χ_e as a function of T_e during the spontaneous oscillation between weak wide and narrow strong ITB in the RS plasma.

5.1.2. Momentum Transport

As discussed previous sections, the plasma rotation is very important to control the plasma confinement and stability. The momentum transport is investigated based on perturbation technique [8]. The modulated ctr-rotation is induced in the peripheral region by the modulated perp. NB injection using the fast ion loss due to the toroidal field ripple. The toroidal momentum diffusivity (χ_ϕ) and the convection velocity (V_{conv}) are evaluated from the amplitude and the phase delay of the modulated part of the toroidal rotation propagated into the inner region. The value of χ_ϕ is ranged from 2 to 25 m^2/s at $r/a \sim 0.6$ by changing absorbed power from 2.4 to 10.7 MW in the L-mode plasmas (I_p = 1.5 MA and B_T = 3.8-4 T), which has good correlation to the ion thermal diffusivity. The negative V_{conv} (inward direction) in the range from 0 to -12 m/s is observed at $r/a \sim 0.6$. In the H-mode plasma, χ_ϕ is smaller by a factor of 2-3 than that in the L-mode plasma.

5.1.3 High Density Limit with High Internal Inductance

In the burning plasma, high density operation is essential. The high density limit is scaled as Geenwald density in tokamaks. However, the underlying physics of the Greenwald density remains an open question. The effects of magnetic shear, which can stabilize pressure driven MHD modes and affect confinement, on the density limit are investigated [24]. High densities exceeding the Greenwald density by a factor of 1.7 is obtained with high internal inductances as high as 2.8. Here, the internal inductance is controlled by I_p ramping down from 1 MA to 0.38 MA with P_{NB}=4.5 MW at B_T = 2.1 T. While the density is beyond the Greenwald limit, confinement performance is kept as good as H_{89PL} = 1.5. The high edge temperature due to the high confinement could retard detachment and consequently increase the density limit.

5.2. Active Control of Neoclassical Tearing Modes

Below no wall ideal limit, suppression of NTM is important to sustain high β_N. NTM suppression techniques have been developed with ECCD at the mode rational surface. The quite different technique from the conventional NTM stabilization is demonstrated with central co-ECCD [25]. The central co-ECCD inside the sawtooth inversion radius enhances sawtooth oscillations [26]. Sawtooth oscillations are considered harmful since a large sawtooth crash can trigger an NTM even at low-β regime. However, evolution of an m/n = 3/2 NTM is suppressed by co-ECCD inside the q = 1 surface. The sawtooth mixing radius reaches the inner side of the m/n = 3/2 magnetic island and frequency of the m/n = 3/2 NTM is modulated by a sawtooth crash, suggesting the possibility of the coexistence of sawtooth oscillations and a small-amplitude m/n = 3/2 NTM without large confinement degradation.

Stabilization of an m/n = 2/1 NTM by ECCD at the q = 2 surface is also demonstrated using the conventional technique with a small ratio of the ECCD current density to the local bootstrap current density ($J_{EC}/J_{BS} \sim 0.5$) [25]. Dependence of the stabilization effect on ECCD location is investigated, where the ratio of $\tilde{B}^{0.5}$ 2 s after the start of EC wave injection (τ_{EC} = 2 s) to that just before the start (τ_{EC} = 0 s) is used

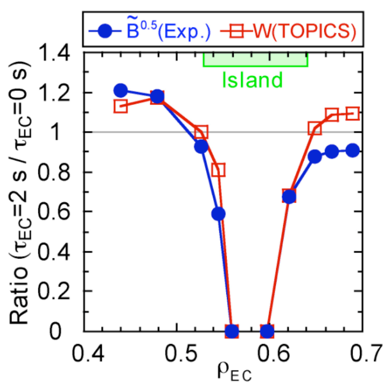

FIG. 13. Dependence of stabilization effect on ECCD location. Island width before EC wave injection is shown in the figure.

for a measure of stabilization effect. It is clarified that an $m/n = 2/1$ NTM can be completely stabilized with the misalignment of the ECCD location less than about half of the island width, and that the $m/n = 2/1$ NTM is destabilized with the misalignment comparable to the island width as shown in Fig. 13. Time-dependent, self-consistent simulation of magnetic island evolution using the TOPICS code [27] shows that the above stabilization and destabilization of an $m/n = 2/1$ NTM are well reproduced with the same set of coefficients of the modified Rutherford equation. The TOPICS simulation has also clarified that EC wave power required for complete stabilization can be significantly reduced by narrowing the ECCD width.

5.3. Energetic Particles

5.3.1. Off-axis NB Current Drive

"Off-axis" NBCD plays an important role in current profile control to keep weak and negative magnetic shear for the advanced tokamak plasma. The current density profile for off-axis NBCD is measured using MSE diagnostic in the ELMy H-mode plasma at $I_p = 0.8$ MA, $B_T = 3.8$ T ($q_{95} = 7.5$) and $\bar{n}_e = 1.4\text{x}10^{19}$ m^{-3} [15]. Figure 14 shows the beam driven current profile (solid line), which is estimated by subtracting ohmic and bootstrap current profiles from the total current profile (dotted line). The peak of the beam driven current is located at $r/a \sim 0.75$. The driven current is estimated to be 0.15 MA (CD efficiency of $0.54\text{x}10^{19}$ AW^{-1}m^{-2}), which is consistent with the decrease in the surface loop voltage.

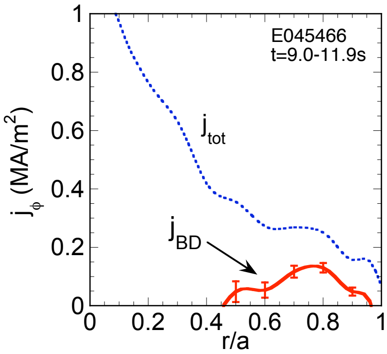

FIG. 14. Measured beam driven current density profile (solid curves) and total current density profile (dotted curves).

5.3.2. Energetic Ions with Alfvén Eigenmodes

In a burning plasma, confinement degradation of alpha particles induced by MHD instabilities such as Alfvén Eigenmodes (AEs) decreases heating efficiency and leads damage on the first wall. Confinement degradation of energetic ions induced by N-NB injection with beam energy of 370-390 keV is investigated [28]. Measured total neutron emission rate (S_n) in the presence of AEs is compared with that predicted by classical theory as shown in Fig. 15. The measured total neutron emission rate is significantly smaller than that predicted by classical theory, indicating confinement degradation of energetic ions from the classical confinement. The confinement degradation is largest in the transition phase from reversed shear induced AEs (RSAEs) to toroidicity induced AEs (TAEs), where the reduction rate from the classical confinement is estimated to be ~ 45%. Line-integrated neutron emission profile indicates that energetic ions are transported from the core region due to these AEs.

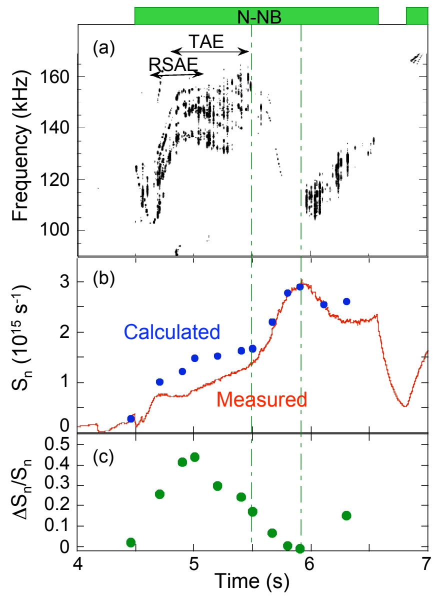

FIG. 15. Comparison between measured neutron emission rate and calculated one.

5.3.3. Observation of Spontaneously Excited Waves Near Ion Cyclotron Range of Frequency

The spontaneously excited waves in the ion cyclotron range of frequency (ICRF) are investigated [29]. Two types of magnetic fluctuations are detected : one is due to high energy D ions from NB injections and the other is due to fusion products (FPs) of ^{3}He and T ions. The frequencies of the fluctuation are just below the cyclotron frequency and its higher harmonics near the outermost magnetic surface. The toroidal wave numbers $k_{//}$ of the excited waves are small for the fluctuations due to D ions and finite value for the fluctuations due to FP-ions. Two types of FP-ion cyclotron emissions are also suggested that the fast wave branch is destabilized due to FP-^{3}He ions and the slow wave branch due to FP-T. These measurements will become a significant diagnostic tool for the fusion reactivity.

6. Studies on Edge/SOL/Divertor Plasmas and Plasma Wall Interactions

In the heating duration longer than ~ 20 s, plasma wall interaction is main issue to sustain the high performance plasmas as discussed in Section 3.1. The plasma control under saturated wall and mechanism of the wall-saturation are investigated. In the long term, erosion and tritium retention finally determine the lifetime of the plasma facing components and operation duration. Carbon erosion/deposition and hydrogen retention are investigated using tile samples picked up from the divertor and main chamber regions and collector probes placed in the shadowed area underneath the divertor. Since transient heat and particle load induced by ELM has an impact upon the erosion, understanding of ELM dynamics is important both inside and outside the separatrix. ELM plasma propagation along and perpendicular to the field lines is investigated using reciprocating probes. High radiation loss operation is effective to reduce the heat load to the divertor plates. Radiation processes are investigated using spectroscopy measurements in the detached divertor plasma for the optimization of the radiative divertor.

6.1. Plasma Control under Saturated Wall

In the discharges with high β_N and high $HH_{98(y,2)}$ discussed in Section 3.1., the divertor pumping rate is lower than the particle fuelling rate from the NB injection due to low recycling and misalignment of the strike points to the pumping slots. With high divertor pumping rate enhanced by increasing recycling and adjusting the strike points to the pumping slots, the density is successfully controlled for ~ 30 s in high-density ELMy H-mode plasmas (I_p = 1.2 MA, B_T = 2.2 T, q_{95} = 3.6) [30] as shown in Fig. 16 (a). The confinement ($HH_{98(y,2)}$ ~ 0.71) comparable to usual H-mode level considering degradation at high density in JT-60U and ELM activity are sustained. At the beginning, a large gas-puffing is applied to increase the density to 2.5×10^{19} m^{-3} (~ $0.64 n_{GW}$) and then the gas-puffing rate gradually decreases to keep the density constant. The wall pumping rate is positive at the beginning, and it decreases to a negative constant ~ 7 s after the start of NB heating, indicating global wall saturation and outgas from the wall. The density is kept constant using the divertor pumping under global wall saturation, even with the outgas. The outgas can be attributed to increase in the divertor-plate temperature as shown in Fig. 16 (b). On the other hand, continuous wall pumping is observed in high density discharges at $\bar{n}_e/n_{GW}$ = 0.82, although injected gas is larger. In these discharges, since the increase in the divertor-plate temperature is small (~ 110 K), it is expected that the outgas is smaller. The continuous wall-pumping can not be explained by co-deposition. The wall-pumping rate seems to increase with the particle flux to the wall. As shown in Fig. 16 (c), X-point MARFE is controlled by the divertor pumping. However, it

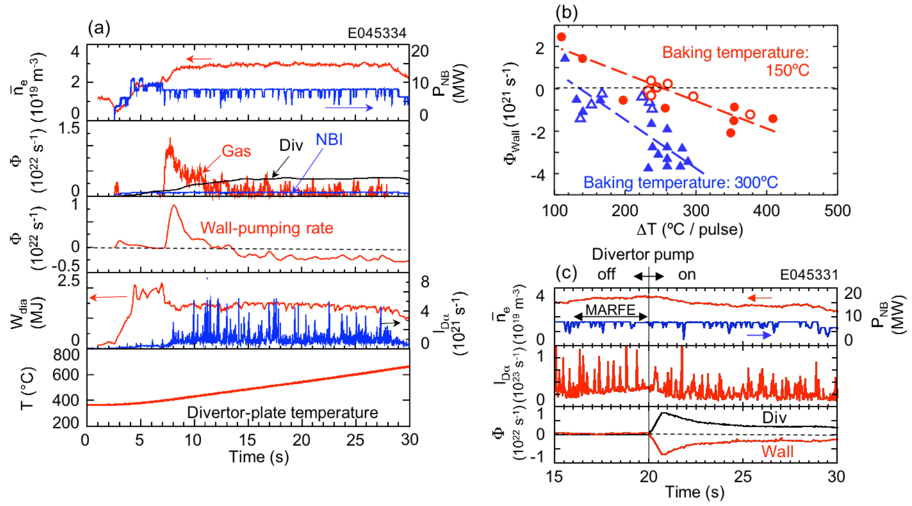

FIG. 16. (a) Waveforms of a long-pulse ELMy H-mode discharge with enhanced divertor pumping. (b) Wall pumping/outgas rate as a function of increase in divertor plate temperature during the pulse. (c) Waveforms of a discharge where divertor pumping is turn on during X-point MARFE.

should be noted that the outgas appeared when the divertor pump is on. Similar decrease in the wall pumping rate (increase in outgas rate) is also observed after the gas-puffing is turned off. These results suggest dynamic equilibrium between particle flux and desorption as a wall pumping mechanism.

6.2. Hydrogen Retention, Carbon Erosion and Co-deposition

Erosion/deposition analyses for the plasma-facing components indicates that local carbon transport to the inboard direction is appreciable in addition to long-path transports [31]. Erosion/deposition patterns of the divertor region are very non-uniform with heavy deposition in the inner divertor (~ 250 μm) and the outer dome wing (~ 120 μm). On the other hand, erosion is dominant in the outer divertor (~ 100 μm) and the inner dome wing (~ 20 μm). The averaged carbon erosion and deposition rates of the divertor surface during the NB heating are estimated to be ~ $10x10^{20}$ and ~ $6x10^{20}$ C atoms/s, respectively, indicating that 40% of the deposition on the divertor region is originated from the main chamber wall. The hydrogen isotopes are co-deposited with carbon and the highest (H+D)/C retention is found to be ~ 0.13 at the deposition dominant area of the outer dome wing (vacuum vessel baking: 570 K). In the plasma-shadowed area underneath the divertor region, ~ 2 μm-thick deposition layer is found (vacuum vessel baking: 420 K), and the averaged deposition rate is estimated to be ~ $8x10^{19}$ C atoms/s, which is significantly lower than that in JET [32]. However, the (H+D)/C retention in the shadowed area is the same level as that observed in JET (~ 0.8). The H+D retention and (H+D)/C in the main chamber wall is estimated to be ~ $10x10^{22}$ atoms/m^2 and ~ 0.16 (vacuum vessel baking: 570 K), respectively. This retention amount significantly contributes to the total retention because of its large surface area.

6.3. ELM Dynamics

In order to reduce transient heat and particle load to the plasma facing components, small or no ELM regimes such as grassy ELM and QH-mode are developed. The grassy ELM frequency is controlled by changing the edge rotation [33]. The ELM frequency increases almost linearly up to 1400 Hz with increasing ctr-rotation and higher ELM frequency of ~ 400 Hz is observed even with zero rotation. The ELM frequency is determined by both ELM crash and inter ELM transport. The inter-ELM energy confinement increases with decreasing edge collisionality and the heat transport in the pedestal region is close to the ion neoclassical transport level in the type I ELM regime [34]. An integrated transport simulation code TOPICS-IB with a stability code for the peeling-ballooning modes and a SOL model has been developed to clarify self-consistent effects of ELMs and SOL on the plasma performance [35]. Experimentally observed collisionality dependence of the ELM energy loss [36] is found to be caused by both the edge bootstrap current and the SOL transport. The ELM stabilities are also investigated using the linear ideal MHD stability code MARG2D [37]. Improvement of stability limit is found with large sharpness, defined in terms of the curvature at the top and bottom of the outer most flux surface, even with same κ and δ.

Since the large (H+D) retention in the main chamber wall is found, particle load to the main chamber wall induced by ELM is investigated. Fast propagation of the ELM plasma is determined both at high-field-side (HFS) and low-field-side (LFS) SOL using reciprocating Mach probes [38]. Large and short (10-20 μs) peaks are found in ELM plasma flux (j_s) mostly at LFS SOL, which is enhanced after each ELM event detected with magnetic probes. Transport dynamics of the first large j_s peak is determined: it propagated to near the LFS main chamber wall with the fast velocity of 1.3-2.5 km/s, as shown in Fig. 17, with large decay length of 9 cm.

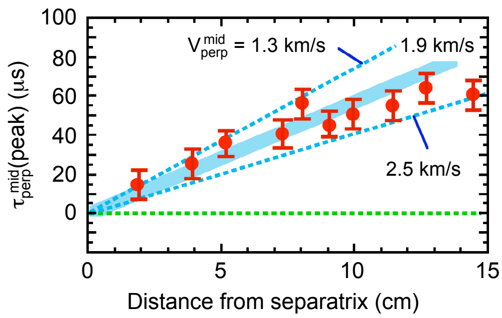

FIG. 17. ELM propagation speed towards LFS main chamber wall.

6.4. Radiation Processes of Impurities and Hydrogen

Understanding of radiation processes is important for achievement of effective heat removal in the divertor plasma. Volumetric recombination of C^{4+} and e^- into C^{3+} around an X-point in the detached plasmas with MARFE is observed [37]. It is found that the radiation power with this recombination process contributes 40% to the total radiation power from the X-point, while the radiation power with the ionization process of C^{3+} into C^{4+} contributes 25%. This result suggests that the radiation power evaluated by spectroscopy is underestimated when only the radiation with ionization process is considered.

7. Summary

Recent JT-60U experiments focus on the extension of the operation regimes and the improvement of the physics understandings for the strong parameter linkage in the advanced tokamak plasmas towards development of steady-state advanced tokamak scenario. The installation of ferritic steel tiles decreases the fast ion loss and enables to access new regimes. High $\beta_N \cdot HH_{98(y,2)}$ of 2.2 with $\beta_N \sim 2.3$ and $HH_{98(y,2)} \sim 1$ is sustained for 23.1 s significantly longer than the current diffusion time ($\sim 12\tau_R$). High β_N of 4.2 exceeding no wall ideal limit is achieved and small critical rotation velocity is found to suppress RWM. NTM stabilization is demonstrated by real time current profile control using LHCD. With small effect of reduction of toroidal field ripple, understanding of strong parameter linkage in the high f_{BS} RS plasmas, physics studies toward burning plasma and plasma-wall interaction are also significantly progressed.

Acknowledgement

The authors would like to acknowledge all people who have contributed to the JT-60U project.

References

[1] TOBITA, K., et al., Fusion Energy 2006, EX/P5-22.
[2] IDE, S. and the JT-60 Team, Nucl. Fusion **45** (2005) S48.
[3] SHIRAI, H., et al., Nucl. Fusion **39** (1999) 1713.
[4] SHINOHARA, K., et al., Fusion Energy 2006, FT/P5-32.
[5] TSUZUKI, K., et. al., Nucl. Fusion **43** (2003) 1288.
[6] SHINOHARA, K., et al., Nucl. Fusion **43** (2003) 586.
[7] KUDO, Y., et al., to be published in Journal of Korean Physical Society (2006).
[8] YOSHIDA, M., et al., Fusion Energy 2006, EX/P3-22.
[9] URANO, H., et al., Fusion Energy 2006, EX/5-1.
[10] KAMADA, Y., et al., Plasma Phys. Control. Fusion **44** (2002) A279.
[11] OYAMA, N., et al., Fusion Energy 2006, EX/1-3.
[12] MIKKELSEN, D. R., Phys. Fluids B **1** (1989) 333.
[13] TAKECHI, M., et al., Fusion Energy 2006, EX/7-1Rb.
[14] REIMERDES, H., et al., 32nd EPS Conference on Plasma Phys. ECA Vol.**29C** (2005) P-5.056.
[15] SUZUKI, T., et al., Fusion Energy 2006, EX/6-4.
[16] FUJITA, T. and JT-60 Team, Phys. Plasmas **13** (2006) 056112.
[17] SAKAMOTO, Y., et al., Fusion Energy 2006, EX/P1-10.
[18] TAKASE, Y., et al., Fusion Energy 2006, EX/1-4.
[19] KURIHARA, K., Fusion Eng. and Design **51-52** (2000) 1049.
[20] IDE, S., et al., Fusion Energy 2006, EX/P1-5.
[21] IDA, K., et al., Fusion Energy 2006, EX/P4-39.
[22] NEUDATCHIN S. V., et al., J. Plasma Fusion Res. **79**, 1218 (2003).
[23] SHIMOMURA, K., submitted to Fusion Engineering and Design.
[24] YAMADA, H., et al., Fusion Energy 2006, EX/P8-8.
[25] ISAYAMA, A., et al., Fusion Energy 2006, EX/4-1Ra.
[26] ISAYAMA, A., et al., J. Plasma Fusion Res. SERIES **5** (2002) 324.
[27] HAYASHI, N., et al., J. Plasma Fusion Res. **80** (2004) 605.
[28] ISHIKAWA, M., et al., Fusion Energy 2006, EX/6-2.
[29] ICHIMURA, M., et al., Fusion Energy 2006, EX/P6-7.
[30] KUBO, H., et al., Fusion Energy 2006, EX/P4-11.
[31] MASAKI, K., et al., Fusion Energy 2006, EX/P4-14.
[32] COAD, J. P., et al., J. Nucl. Mater. **290-293** (2001) 224.
[33] OYAMA, N., et al., submitted to Plasma Phys. Control. Fusion
[34] URANO, H., et al., Phys. Rev. Lett. **95** (2005) 035003.
[35] HAYASHI, N., et al., Fusion Energy 2006, TH/4-2.
[36] LOARTE, A., et al., Plasma Phys. Control. Fusion **45** (2003) 1549.
[37] AIBA, N., et al., Fusion Energy 2006, TH/P8-1.
[38] ASAKURA, N., et al., Fusion Energy 2006, EX/9-2.
[39] NAKANO, T., et al., Fusion Energy 2006, EX/P4-19.